Neurosci. Bull. February, 2020, 36(2):110–120
https://doi.org/10.1007/s12264-019-00418-0

www.neurosci.cn
www.springer.com/12264

ORIGINAL ARTICLE

MiR-125a-5p Regulates Vitamin D Receptor Expression in a Mouse Model of Experimental Autoimmune Encephalomyelitis

Han-Chun Long[2,4] · Rui Wu[3] · Chun-Feng Liu[2,3] · Fei-Long Xiong[2,4] · Zu Xu[1] · Dian He[1] · Yi-Fan Zhang[1] · Bing Shao[1] · Ping-An Zhang[3] · Guang-Yin Xu[3] · Lan Chu[1,2]

Received: 19 February 2019 / Accepted: 8 May 2019 / Published online: 19 August 2019

Abstract Multiple sclerosis (MS) is a chronic and incurable autoimmune neurodegenerative disease of the central nervous system. Although the symptoms of MS can be managed by vitamin D3 treatment alone, this condition cannot be completely eradicated. Thus, there might be unknown factors capable of regulating the vitamin D receptor (VDR). Genome-wide analysis showed that miRNAs were associated with VDRs. We sought to determine the role and mechanism of action of miRNA-125a-5p and VDRs in a model of MS, mice with experimental autoimmune encephalomyelitis (EAE), which was induced by myelin oligodendrocyte glycoprotein 35–55 peptides. EAE mice showed decreased mean body weight but increased mean clinical scores compared with vehicle or control mice. And inflammatory infiltration was found in the lumbosacral spinal cord of EAE mice. In addition, VDR expression was significantly lower while the expression of miR-125a-5p was markedly higher in the spinal ventral horn of EAE mice than in vehicle or control mice. Importantly, activation of VDRs by paricalcitol or inhibition of miR-125a-5p by its antagomir markedly decreased the mean clinical scores in EAE mice. Interestingly, VDR and miR-125a-5p were co-localized in the same neurons of the ventral horn. More importantly, inhibition of miR-125a-5p remarkably blocked the decrease of VDRs in EAE mice. These results support a critical role for miR-125a-5p in modulating VDR activity in EAE and suggest potential novel therapeutic interventions.

Keywords Multiple sclerosis · Experimental autoimmune encephalomyelitis · Vitamin D receptor · MiR-125a-5p · Myelin oligodendrocyte glycoprotein 35–55 peptides

Introduction

Multiple sclerosis (MS) is a genetically [1–3] and immunologically complex disease defined by both myelin loss and neurodegeneration. It is characterized by infiltration of T lymphocytes and monocytes, inflammatory mediators, loss of oligodendrocytes, formation of reactive astrocytes, and axonal injury and loss [4–7]. The therapeutic interventions for MS are very limited and poorly effective [8], resulting in repeated attacks of the condition [9, 10]. Moreover, the molecular mechanisms underlying MS are poorly understood. Therefore, investigation of the pathogenic mechanism of MS is essential. The experimental autoimmune encephalomyelitis (EAE) mouse is a useful experimental model of MS in which inflammation provokes neurological and pathological symptoms similar to those of MS patients [4].

A growing body of evidence has pointed out that environmental factors might play a major role in MS

Han-Chun Long and Rui Wu have contributed equally to this work.

✉ Guang-Yin Xu
guangyinxu@suda.edu.cn

✉ Lan Chu
chulan8999@yeah.net

1 Department of Neurology, The Affiliated Hospital of Guizhou Medical University, Guiyang 550001, China

2 Department of Neurology, The Second Affiliated Hospital of Soochow University, Suzhou 215008, China

3 Institute of Neuroscience, Soochow University, Suzhou 215123, China

4 Department of Neurology, The Affiliated Xingyi City Hospital of Guizhou Medical University, Xingyi 562400, China

[11, 12]. Studies have shown that deficiency of vitamin D3 (D3) increases the incidence of EAE. Direct immunomodulatory effects of D3 on cells of the central nervous system (CNS), including astrocytes [13] and microglia [14], have recently been reported, and the D3 signals in a variety of immune cells are mediated by the vitamin D receptors (VDRs) [15–17]. The regulatory role of VDRs in adaptive immune responses also includes an inhibitory effect on dendritic cell maturation and differentiation [18, 19]. Vitamin D analogs like paricalcitol (PC) attenuate the inflammatory process and preserve the myelin sheath [20, 21]. However, the regulation of VDR expression and its involvement in MS are still unclear.

MicroRNAs (mRNAs) are small non-coding RNAs that regulate gene expression and stabilize the translation of mRNAs. They are involved in many biological and pathological processes such as development, functional dysregulation, differentiation, regeneration, and ontogenesis [2, 22–24], as well as several autoimmune diseases including MS [25, 26]. However, in autoimmune diseases, promising miRNA candidates for therapeutic development remain severely limited. MiRNAs exert their functions by binding to the 3' untranslated regions (UTRs) of their target mRNAs, thus promoting mRNA degradation or repressing protein translation [27, 28]. However, the regulation of VDR expression by miRNAs in MS remains unclear. According to bioinformatics analysis (Targetscan and miRNA.org), miR-125-5p can bind to the 3' UTR of VDR mRNA. MiR-125a-5p has been confirmed to be functionally relevant in the context of immune cell activation, and inflammation – particularly in the settings of rheumatoid arthritis, neuroinflammation [29], and autoimmune diseases [30], but its role in MS remains unclear.

Based on these findings, we focused on roles of miR-125a-5p and VDRs. We hypothesized that miR-125a-5p regulates VDR expression in the spinal ventral horn in a mouse model of EAE.

Materials and Methods

Animals

Adult female C57BL/6 mice (n = 60, 8–12 weeks old, 18–20 g) were housed at a constant temperature of 24 ± 2 °C, 40%–60% relative humidity, and a 12-h light-dark cycle in a clean-level animal facility at the Experimental Animal Center of Soochow University. Animals were provided by the Animal Care and Use Committee of Soochow University. Food and water were given *ad libitum*. Animals were used for behavioral experiments and detection of molecular biological changes. All procedures were performed according to the guidelines of the International Association for the Study and the Animal Care Committee of the Soochow University and were approved.

Experimental Design

Mice were separated into the following groups (n = 60 in total, Fig. 1): 1. Control group (CON, n = 10), mice did not receive any injection; 2. Vehicle group (Vehicle, n = 10), each mouse was injected with 0.1 mL complete Freund's adjuvant (CFA) (Sigma-aldrich, St. Louis, MO) only; 3. EAE group (EAE, n = 10), each mouse was immunized by injecting 0.1 mL myelin oligodendrocyte glycoprotein (MOG) 35–55 peptide (A Peptide Co., Ltd, Shanghai, China) subcutaneously – this formulation comprised 8 mg MOG 35–55 peptides emulsified in 4 mL CFA at a final concentration of 2 mg/mL, and contained 4 mg/mL of mycobacterium tuberculosis (Kaichuang, Shijiazhuang, China). This was followed by intraperitoneal injection of 0.1 mL of pertussis toxin (300 ng/0.1 mL, Sigma) in phosphate buffered saline (PBS) 1 h after MOG injection. A second identical dose of pertussis toxin was given 48 h after immunization (by intraperitoneal injection). 4. EAE + PC group (n = 10), mice were anesthetized by isoflurane and PC was administered by intraperitoneal injection (0.1 mL, 1 μg/kg). 5. EAE + miR-125a-5p antagomir (n = 10), MOG-injected mice were given miR-125a-5p antagomir or antagomir NC (10 μL, 200 nmol) (n = 10) daily after EAE induction [31].

The total number of animals used was 72, but 12 were excluded (rule out models that are not successful), leaving 60.

EAE severity was determined by body weight and clinical scores. Body weight and symptoms were recorded daily. The clinical scores were assigned according to the following scale: Grade 0, no clinical signs; Grade 1, tail paralysis; Grade 2, abnormal gait; Grade 3, hind limb paralysis; Grade 4, complete paralysis; Grade 5, death or euthanasia with scoring intervals of 0.5 as described previously [32, 33]. Twenty-one days after EAE induction, mice were sacrificed and spinal cord tissue was collected and stored at − 80 °C for further analyses.

Hematoxylin and Eosin Staining

Histopathological analysis was performed on day 21 after EAE induction. After euthanasia, lumbar spinal cord specimens were removed and fixed in 10% neutral buffered formalin. The tissue was dehydrated in graded ethanols and embedded in Paraplast Plus (McCormick, St. Louis, MO). Serial sections were cut at 10 μm and stained with hematoxylin and eosin (HE). Five photomicrographs were

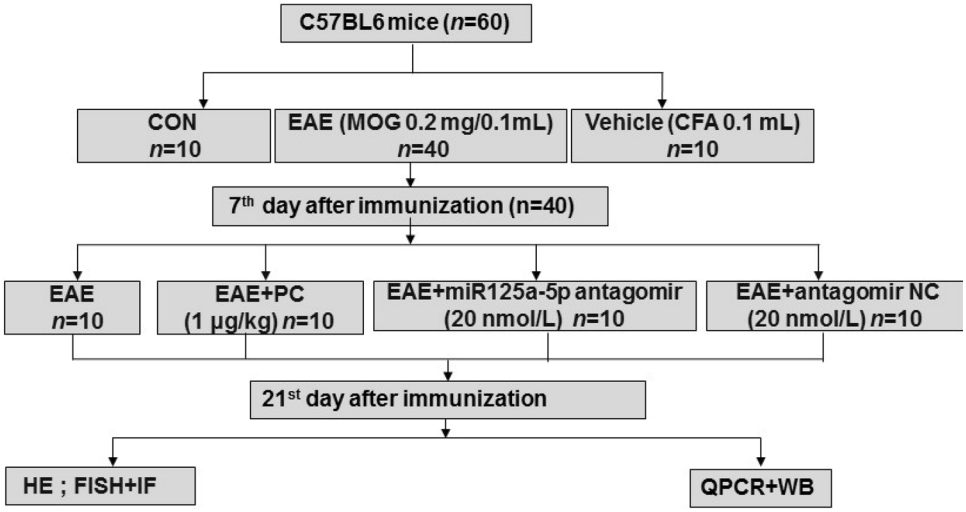

Fig. 1 Flowchart of the experimental design.

captured from each animal with a Nikon microscope (Olympus, Shinjuku-ku, Tokyo, Japan). CNS inflammation was assessed using a semi-quantitative scoring system according to the following previously-described criteria [34]: 0, no infiltrates; 1, partial meningeal infiltration; 2, pronounced meningeal infiltration; 3, pronounced meningeal and some parenchymal infiltration.

Immunofluorescence

Mice were deeply anesthetized by isoflurane inhalation and then transcardially perfused with normal saline and 4% paraformaldehyde (Sinopharm Chemical Reagent Co. Ltd, Shanghai, China). Next, the lumbar enlargement was removed, post-fixed for 2 h with paraformaldehyde, and then dehydrated successively in 10%, 20% and 30% sucrose (dissolved in PBS; Sinopharm Chemical Reagent Co. Ltd.) until the tissue sank. The tissue was embedded in optimal cutting temperature compound (Sakura, Tokyo, Japan) and stored at – 80 °C until sectioning. The tissue was cut at 10 μm on a freezing microtome (Leica, Wetzlar, Germany). For immunofluorescence, the sections were washed with PBS, blocked with 2% bovine serum albumin in PBS for 2 h, and then incubated overnight with primary antibodies against VDR (1:1000, Santa Cruz Biotechnology, CA, USA), NeuN (1:50, Merck Millipore, MA, USA), GFAP (1:300, Millipore), and CD11b (1:200, Abcam, Cambridge, UK) at 4 °C overnight. The sections were washed three times with PBS for 5 min, and then incubated with the secondary antibodies Alexa Fluor488 (1:500, Molecular Probes, New York, USA) and Alexa Fluor555 (1:100, Molecular Probes) for 2 h at room temperature (RT). Primary antibodies were omitted to provide negative controls.

Fluorescence *In Situ* Hybridization (FISH)

FISH was performed with an enhanced sensitivity ISH detection Kit I (POD, Boster, Wuhan, China). A locked nucleic acid probe complementary to miR-125a-5p was labeled with 5′ and 3′-digoxigenin and synthesized by Exiqon (Woburn, MA, USA). The slides were incubated in blocking buffer for 30 min at RT before they were pre-hybridized for 2 h at 37 °C, and then exposed to a 1 μg/mL probe in 60–120 μL of hybridization mixture that was added to each slide and incubated overnight at 37 °C. After washing with 2 × Saline Sodium Citrate (SSC), 0.5 × SSC, and 0.2 × SSC, the slides were blocked in blocking solution, biotinylated mouse anti-digoxin was added and left for 1–2 h, then after 3 washes with 0.5 mol/L PBS for 5 min each, the slides were incubated with POD-CY3 (1:100) for 1 h (Boster). The slides were blocked with 2% bovine serum albumin in PBS for 2 h and then incubated overnight with primary antibodies and fluorogenic secondary antibodies. All images were captured with a confocal microscope (Leica, TCS SP8).

Western Blot

Spinal ventral horns isolated from control and EAE mice were homogenized by ultrasonication in lysate. The re-suspended pellets were kept on ice for 2 h, centrifuged at 15,000 rpm for 30 min at 4 °C, and the supernatant retained to estimate proteins. The quantity of protein was determined with a BCA protein assay kit (MultiSciences, Hangzhou, China). After denaturation in a water bath at 75 °C for 10 min, protein samples (40 μg) were loaded onto 10% sodium dodecyl sulfate polyacrylamide gels (Bio-Rad, Hercules, CA) and transferred onto polyvinylidene difluoride membranes (Millipore). After transfer, the membranes were blocked with Tris-HCl buffer solution

(TBS) (50 mmol/L Tris-HCl, 133 mmol/L NaCl, pH = 7.4) containing 5% non-fat dried milk for 2 h at RT, and incubated overnight at 4 °C with the following specific antibodies: VDR (1:1000; Santa Cruz Biotechnology, USA) and GAPDH (1:2000, Santa Cruz Biotechnology). Then, membranes were washed in TBST (TBS containing 0.5% Tween) and incubated with horseradish peroxidase-conjugated anti-mouse (1:2000, Multi sciences, Hangzhou, China) or anti-rabbit IgG secondary antibody (1:2000, Jackson ImmunoResearch Laboratories, PA, USA) for 2 h at RT. Then, protein bands were quantified by enhanced chemiluminescence (Tanon, Shanghai, China) followed by optical density analysis. All images were captured using ImageJ software (Bio-Rad, CA, USA).

Real-Time Quantitative PCR (qPCR)

According to the manufacturer's instructions, RNA was extracted with TRIzol reagent (Ambion, Shanghai, China). The first-strand cDNA of the VDR was synthesized and analyzed from total RNA using a standard protocol with a reverse transcription kit (Transgen Biotech, Beijing, China). The PCR denaturation temperature curve was composed of 40 cycles at 95 °C for 15 s, with an annealing and elongation reaction at 60 °C for 1 min. The primers used for qPCR were utilized by Sangon Biotech (Shanghai, China). U6 was used as an internal control for miRNA. The primers used in this study were as follows:

GAPDH-F: 5′-GGTTGTCTCCTGCGACTTCA-3′;
GAPDH-R: 5′-TGGTCCAGGGTTTCTTACTCC-3′;
mmu-miR-125b-5p-F: 5′-CGCGTCCCTGAGACCCTAAC-3′;
mmu-miR-125b-5p-RT: 5′-GTCGTATCCAGTGCAGGGTCCGAGGTATTCGCACTGGATACGACTCACAA-3′;
mmu-miR-351-5p-F 5′-GTCCCTGAGGAGCCCTTTG-3′;
mmu-miR-351-5p-RT: 5′-GTCGTATCCAGTGCAGGGTCCGAGGTATTCGCACTGCATACGACCAGGCT-3′;
mmu-miR-125a-5p-F: 5′-GCGTCCCTGAGACCCTTTAAC-3′;
mmu-miR-125a-5p-RT: 5′-GTCGTATCCAGTGCAGGGTCCGAGGTATTCGCACTGGATACGACTCACAG-3′;
U6-F: 5′-AGAGAAGATTAGCATGGCCCCTG-3′;
U6-R: 5′-AGTGCAGGGTCCGAGGTATT-3′;
U6-RT: 5′-GTCGTATCCAGTGCAGGGTCCGAGGTATTCGCACTGGATACGACAAAAAT-3′;
VDR-F: 5′-GCAGCGTAAGCGAGAGATGAT-3′;
VDR-R: 5′-AGGGGGTGTACAGATCAGAGTTTG-3′.
Common primer downstream of stem loop: 5′-AGTGCAGGGTCCGAGGTATT-3′.

Levels of gene expression are presented as relative fold difference using the method of the delta-delta threshold ($2^{-\Delta\Delta Ct}$).

Statistical Analysis

All results are expressed as the mean ± SEM. Prior to analysis, all data were tested for normality. When the comparisons involved two means, Student's *t*-test was used. When multiple comparisons were involved, a single factor analysis of variance (ANOVA) or Friedman ANOVA was first performed to obtain a global test of the null hypothesis. If the overall *P*-value (alpha value) of the null hypothesis test was $P < 0.05$, subsequent comparison of different groups was conducted using the Dunn's subsequent test. The Mann–Whitney test was used when the means were not normally distributed. When an alpha value of $P < 0.05$ was evident, the comparison was considered statistically significant. Quantitative statistical data were analyzed using Prism software for multi-group comparisons (Version 8, GraphPad-Prism, San Diego, CA).

Results

Mean Clinical Scores are Higher and Body Weight Lower in EAE Mice

From the day of administration, EAE animals were less active and responsive, with a weak tail and rough unkempt fur. By comparing the mean clinical scores of the three groups, we found that the scores in the EAE group were significantly higher, but their body weights were clearly lower than the control and vehicle groups from day 7 after immunization ($n = 6$). The mean clinical score of the control and vehicle groups was 0 ± 0 on all days, and body weight gradually increased from day 0 to 21 ($n = 6$). However, the mean clinical score of the EAE group gradually increased (Fig. 2A), and their body weight gradually decreased from day 0 to 21 (Fig. 2B).

Inflammatory Infiltration in Lumbosacral Spinal Cord of EAE Mice

On day 21 post-immunization, the lumbosacral spinal cord was removed from mice of each group, paraffin sectioned, and stained with HE (Fig. 2C, D). The results showed that there was no phenomenon of "vascular cuff" and inflammatory infiltration in control mice (Fig. 2C, left). However, diffuse inflammatory infiltration and a phenomenon of "vascular cuff" were found in EAE mice (Fig. 2C, right). Pathological scores were 0 ± 0 ($n = 3$) in control mice and

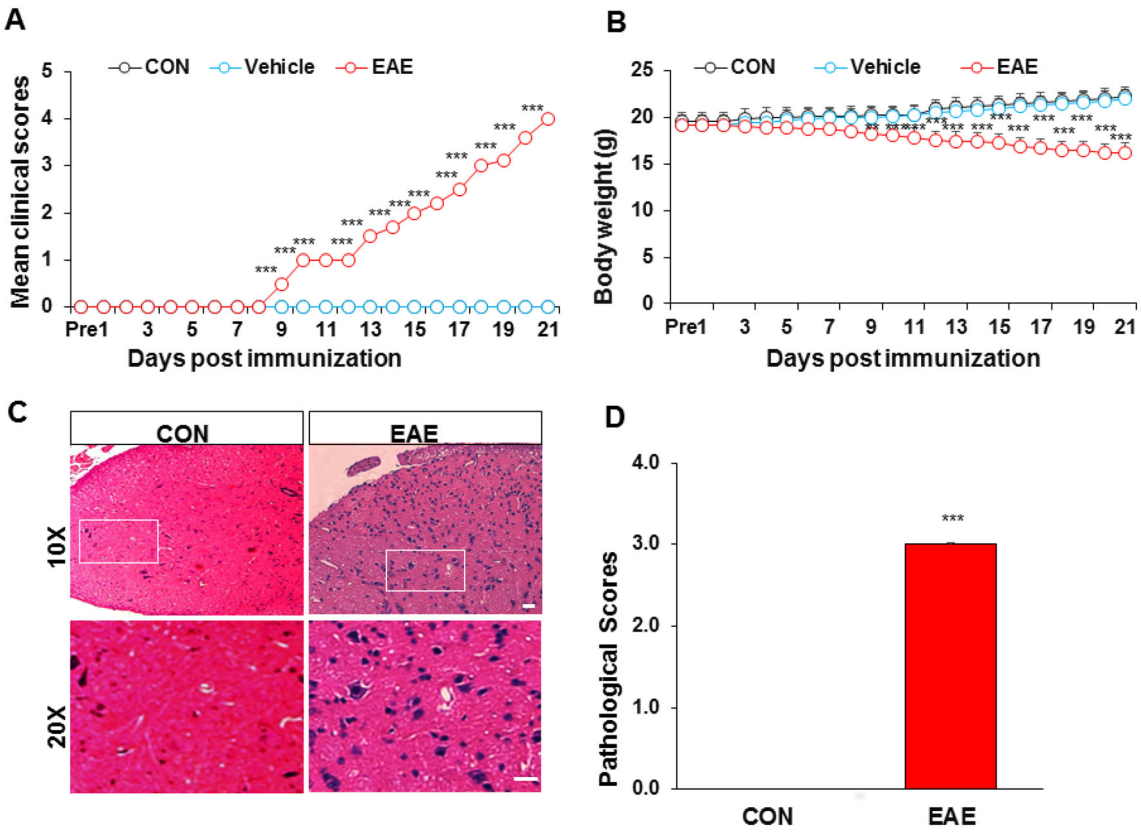

Fig. 2 Changes in mean clinical scores, body weight, and HE staining in EAE mice. **A** The mean clinical score was higher in the EAE than in the control (CON) and vehicle groups ($n = 6$, $^{***}P < 0.001$, two-way ANOVA). **B** The body weight of EAE mice decreased gradually, while that of control and vehicle mice increased ($n = 6$, $^{**}P < 0.01$, $^{***}P < 0.001$, two-way ANOVA). **C**, **D** Control mice had no phenomenon of "vascular cuff" or inflammatory infiltration. However, EAE mice showed diffuse inflammatory infiltration, some of which showed a phenomenon of "vascular cuff". $n = 3$; $^{***}P < 0.001$, Mann–Whitney test; scale bars, 50 μm.

significantly higher at 3.00 ± 0.02 ($n = 3$) in EAE mice (Fig. 2D).

VDR Expression is Lower in the Ventral Horn of EAE Mice

VDR expression in the ventral horn was assessed by qPCR and Western blot. The results showed that the relative mRNA levels of VDR were 1.00 ± 0.24 ($n = 4$) in control mice, 0.97 ± 0.16 ($n = 4$) in vehicle mice, and 0.11 ± 0.04 ($n = 4$) in EAE mice. Statistical analysis showed that the VDR mRNA in EAE mice was markedly lower than that in control or vehicle mice (Fig. 3A). Western blots showed that the relative protein levels of VDR were 0.83 ± 0.07 ($n = 4$) in control mice, 0.67 ± 0.02 ($n = 4$) in vehicle mice, and 0.43 ± 0.01 ($n = 4$) in EAE mice, and VDR expression was significantly lower in EAE mice than in age-matched control or vehicle mice (Fig. 3B).

VDR is Mainly Expressed in Neurons of the Ventral Horn

Localization of VDRs in the ventral horn of EAE mice was determined by immunofluorescence staining. As shown in Fig. 4, cells were stained red by NeuN (a marker of neurons), CD11b (a marker of microglia), or GFAP (a marker of astrocytes) (Fig. 4A, D, G), and VDR-positive cells were stained green (Fig. 4B, E, H). The merged images showed that VDR was mainly expressed in neurons (Fig. 4C), but not in microglia (Fig. 4F) or astrocytes (Fig. 4I).

EAE Enhances the Expression of MiR-125a-5p in the Ventral Horn

Using bioinformatics prediction software (Targetscan and miRNA.org), we found that miR-125a-5p, miR-125b-5p, and miR-351-5p targeted to the 3' UTR of VDR mRNA. To test whether these selected miRNAs are involved in EAE, qPCR was used to assess their expression in the lumbar enlargement. The relative miRNA levels of miR-

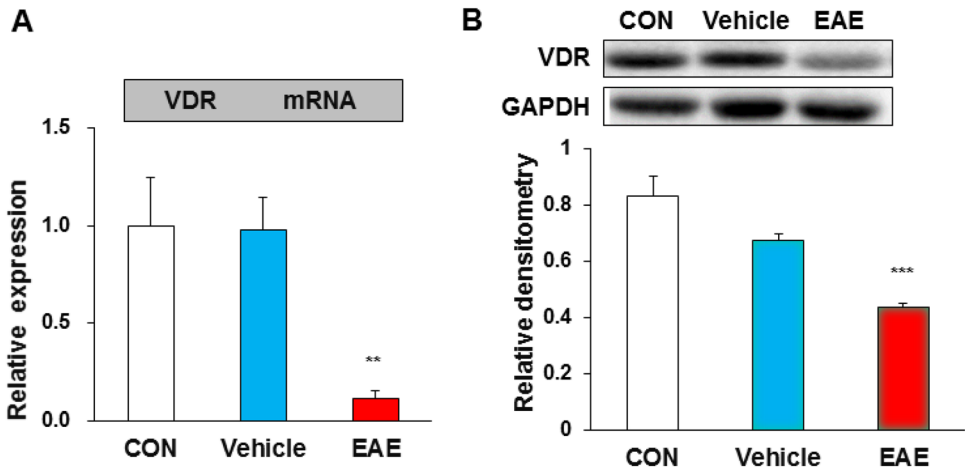

Fig. 3 VDR expression was decreased in the ventral horn of EAE mice. VDR expression assessed by qPCR and Western blot. **A** The VDR mRNA level in EAE mice was markedly lower than in control (CON) or vehicle mice ($n = 4$, $^{**}P < 0.01$, one-way ANOVA). **B** Western blots and statistics showing that VDR expression was lower in EAE than in age-matched control or vehicle mice ($n = 4$, $^{***}P < 0.001$, one-way ANOVA).

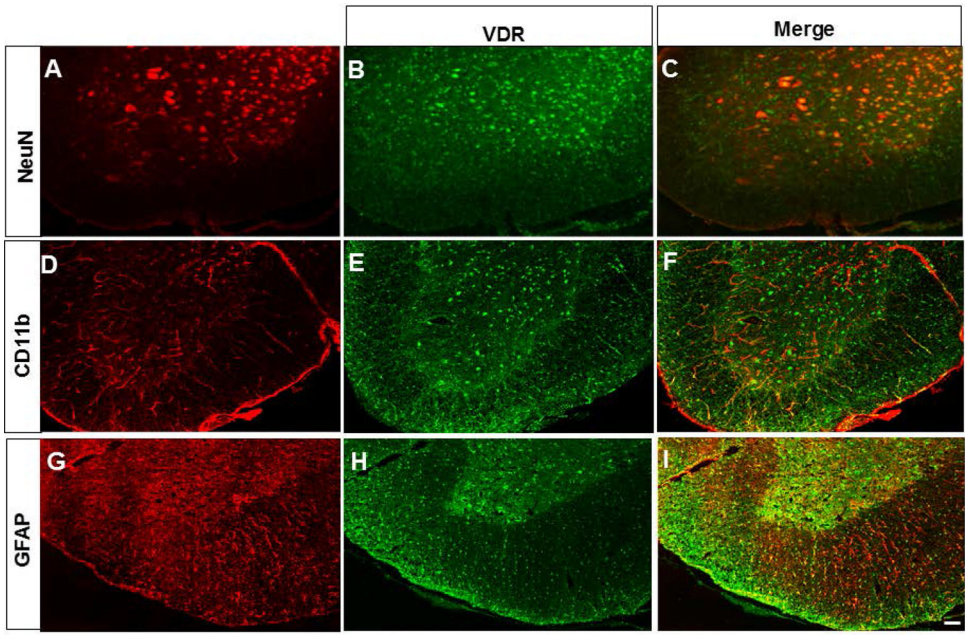

Fig. 4 VDR was mainly expressed in neurons of the ventral horn. (**A**, **D**, **G**) Cells stained red by NeuN (a marker of neurons), CD11b (a marker of microglia), or GFAP (a marker of astrocytes), and (**B**, **E**, **H**) VDR-positive cells stained green. The merged images show that VDR was mainly expressed in neurons (**C**), but not in microglia (**F**), or astrocytes (**I**) in the ventral horn of EAE mice. Scale bar, 50 μm.

125a-5p were 1.00 ± 0.87 in control, 1.32 ± 1.04 in vehicle, and 4.76 ± 0.54 in EAE mice ($n = 4$ for each). Statistical analysis showed significantly higher miRNA levels of miR-125a-5p in EAE than that in control or vehicle mice (Fig. 5A). The relative miRNA levels of miR-125b-5p were 1.00 ± 0.50, 2.02 ± 0.57, and 0.74 ± 0.19 ($n = 4$ for each), respectively. The same values for miR-351-5p were 1.00 ± 0.31, 1.78 ± 0.34, and 1.97 ± 0.25 ($n = 4$ for each). There were no significant differences in the miRNA levels of miR-125b-5p and miR-351-5p for EAE compared with control or vehicle mice (Fig. 5B, C). These results suggested that the expression of miR-125a-5p is enhanced in the ventral horn of EAE mice, but miR-125b-5p and miR-351-5p are unchanged.

MiR-125a-5p is Mainly Expressed in Neurons of the Ventral Horn

FISH was conducted to detect miR-125a-5p localization. Cells were stained green by NeuN (a marker of neurons, Fig. 6A), CD11b (a marker of microglia, Fig. 6E), or GFAP (a marker of astrocytes, Fig. 6I), while miR-125a-5p-positive cells were stained red (Fig. 6B, F, J), and DAPI stained nuclei blue (Fig. 6C, G, K). The merged images showed that miR-125a-5p was mainly expressed in neurons (Fig. 6D), but not in microglia (Fig. 6H) or astrocytes (Fig. 6L).

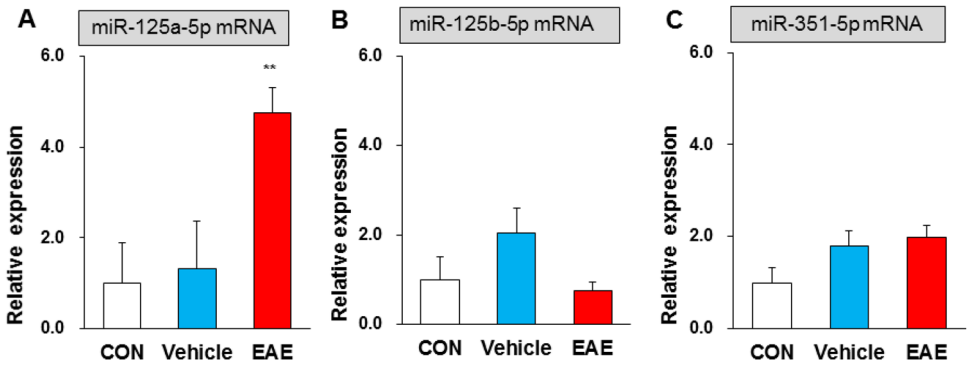

Fig. 5 EAE enhanced the expression of miR-125a-5p in the ventral horn. **A** Statistical analysis showing significantly higher miRNA levels of miR-125a-5p in EAE than in control (CON) and vehicle mice ($n = 4$, $^{**}P < 0.01$, one-way ANOVA). **B**, **C** Statistical analysis showing no significant differences in miRNA levels of miR-125b-5p and miR-351-5p for EAE compared with control and vehicle mice ($n = 4$, $P > 0.05$, one-way ANOVA).

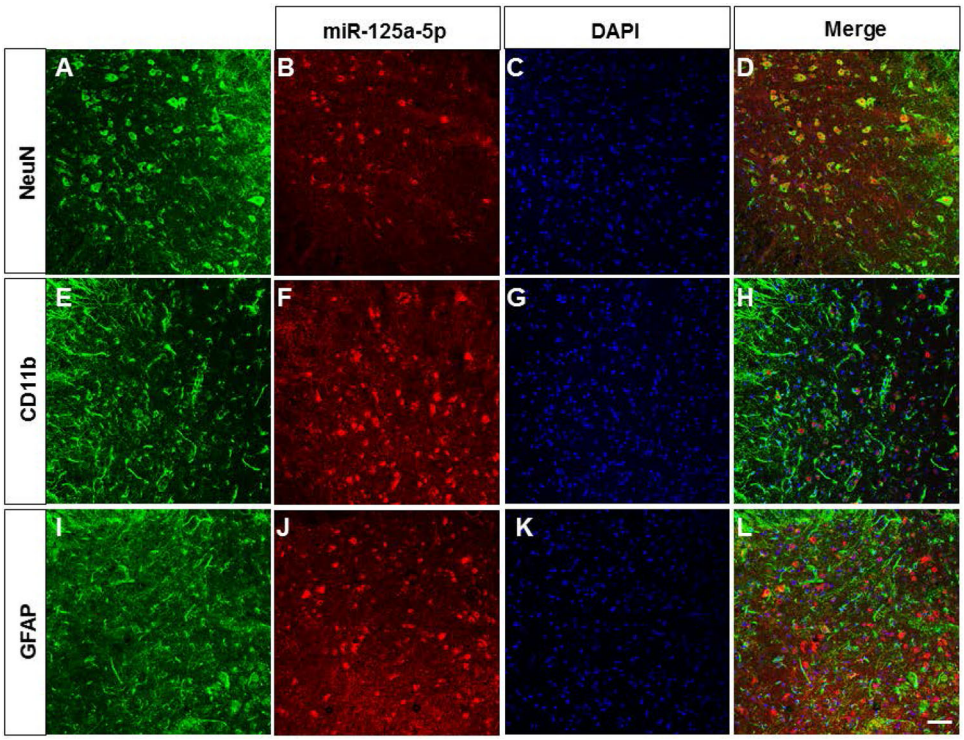

Fig. 6 MiR-125a-5p was mainly expressed in neurons of the ventral horn. The merged images showed that miR-125a-5p was mainly co-expressed with NeuN (**A**–**D**). MiR-125a-5p was not co-labelled with CD11b (**E**–**H**) or GFAP (**I**–**L**) in the ventral horn of EAE mice. Scale bar, 50 μm.

MiR-125a-5p and VDRs are Co-Localized

A precondition of the reaction between miR-125a-5p and VDRs is that they must be co-expressed in the same cell, so we used FISH to detect their co-localization. MiR-125a-5p-positive cells were stained red (Fig. 7A), VDR-positive cells were stained green (Fig. 7B), and DAPI stained nuclei blue (Fig. 7C). The merged results for VDRs and miR-125a-5p showed that they were co-expressed in the same neurons (Fig. 7D). The results for merged DAPI and miR-125a-5p showed that miR-125a-5p was mainly expressed in the cytoplasm (Fig. 7E, F).

Agonist of VDR or miR-125a-5p Antagomir Attenuates the Symptoms of EAE Mice

To verify the involvement of VDR in EAE mice, we used PC, an efficient agonist of VDR. On day 9 after PC treatment, the mean clinical score of EAE mice was lower and remained at a lower level than untreated EAE mice (Fig. 8A). Similarly, by day 9 after intraperitoneal injection of PC, the mean body weight of EAE mice gradually increased (Fig. 8B). These data suggested that VDR is involved in the MS of EAE mice. To further confirm the involvement of miR-125a-5p in MS, we used its antagomir. As expected, the miR-125a-5p antagomir (intrathecal

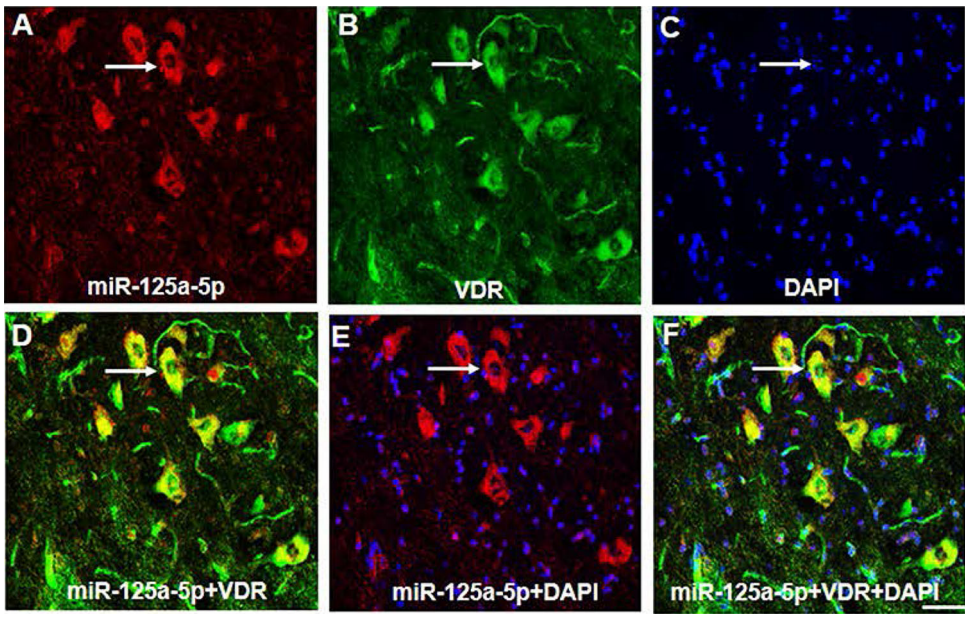

Fig. 7 MiR-125a-5p and VDR were co-localized. **A**, **B** MiR-125a-5p-positive cells were stained red (**A**), and VDR-positive cells were stained green (**B**). **C** DAPI stained the nuclei blue. **D** VDR and miR-125a-5p merged showing that both were co-expressed in the same neurons. **E** DAPI and miR-125a-5p merged showing that miR-125a-5p was mainly expressed in the cytoplasm. **F** Merged images showing that miR-125a-5p and VDR were mainly co-expressed in the cytoplasm of EAE mice. Scale bar, 25 μm. Arrow indicates a representative cell which co-expressed miR-125a-5p dyed in red and VDR dyed in green.

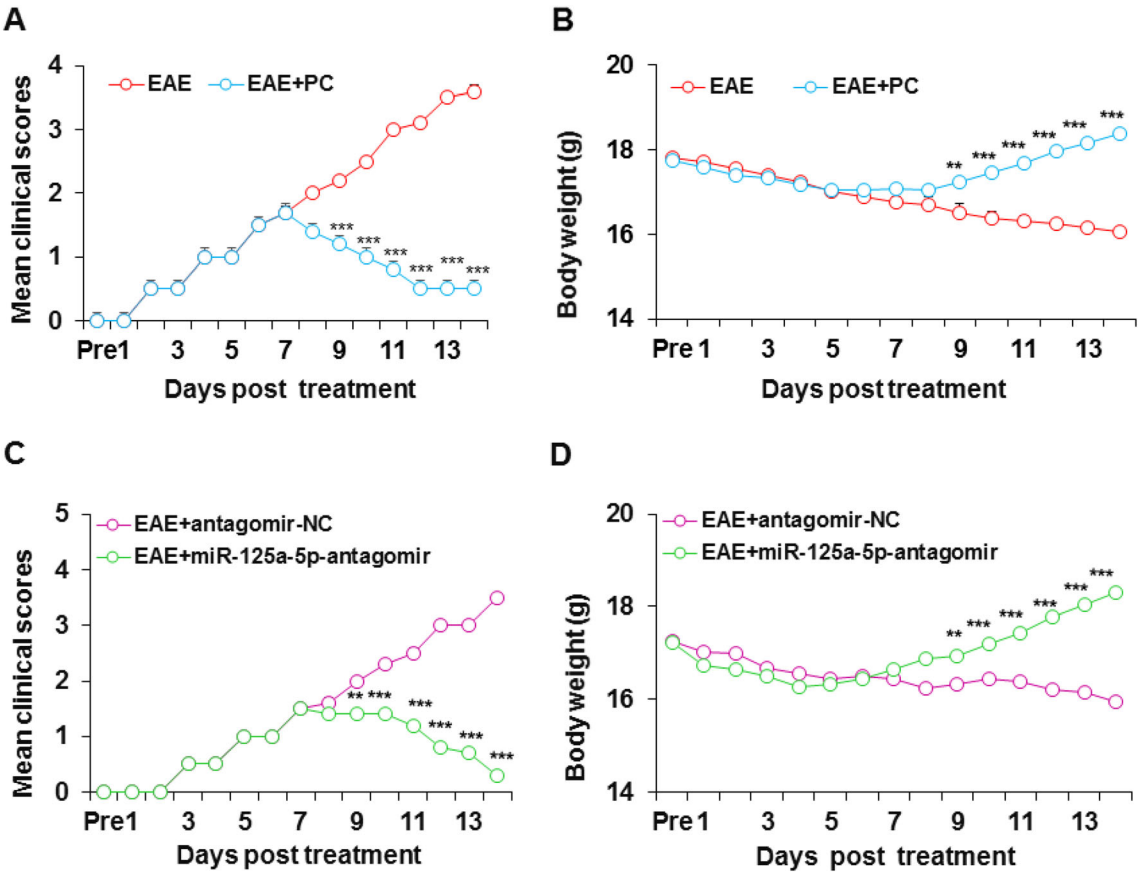

Fig. 8 Agonist of VDR or miR-125a-5p antagomir attenuated the symptoms of EAE mice. **A** Mean clinical scores of EAE mice were lower from day 9 after PC treatment than in untreated EAE mice ($n = 6$, $^{***}P < 0.001$, two-way ANOVA). **B** The body weight of mice in the EAE + PC group gradually increased from day 9 after PC treatment, while the body weight of the untreated EAE group gradually decreased ($n = 6$, $^{**}P < 0.01$,$^{***}P < 0.001$, two-way ANOVA). **C** Intrathecal injection of miR-125a-5p antagomir decreased mean clinical scores of EAE mice and attenuated the paralysis ($n = 6$, $^{**}P < 0.01$, $^{***}P < 0.001$, two-way ANOVA). **D** Intrathecal injection of miR-125a-5p antagomir increased the body weight of EAE mice ($n = 6$, $^{**}P < 0.01$, $^{***}P < 0.001$, two-way ANOVA).

injection) significantly improved the clinical scores (Fig. 8C) and body weight (Fig. 8D) of EAE mice compared with the antagomir-NC group.

MiR-125a-5p Antagomir Reverses the Decreased VDR Expression and Pathogenesis in EAE Mice

To determine how VDRs are regulated by miR-125a-5p, we assessed the mRNA and protein expression levels of VDR after intrathecal injection of miR-125a-5p antagomir or antagomir-NC. QPCR showed that the relative mRNA levels of VDR were 1.00 ± 0.92 ($n = 4$, EAE), 1.01 ± 0.67 ($n = 4$, antagomir-NC), and 12.62 ± 0.14 ($n = 4$, miR-125a-5p antagomir). Statistical analysis suggested that the VDR mRNA level was significantly higher in EAE mice after intrathecal injection of the miR-125a-5p antagomir than in the antagomir-NC and EAE groups (Fig. 9A). Western blot assays showed that VDR protein expression in EAE mice was significantly increased after intrathecal injection of the miR-125a-5p antagomir compared with the antagomir-NC or EAE groups (Fig. 9B). The relative densitometry of VDR was 0.34 ± 0.03 ($n = 4$) in EAE mice, 0.33 ± 0.00 ($n = 4$) in EAE mice treated with antagomir-NC, and 0.75 ± 0.06 ($n = 4$) in EAE mice treated with miR-125a-5p antagomir. These results suggested that miR-125a-5p targets VDRs in the mouse model of EAE.

Discussion

Vitamin D and its receptor VDR are closely associated with the development and appearance of autoimmune diseases, especially in MS [19, 35–37]. Although the symptoms of MS can be managed by vitamin D3 (D3) treatment alone, this condition cannot be completely eradicated. Thus, we suspected that there might be some unknown factors capable of regulating VDRs. The extensive involvement of miRNAs in human diseases has strengthened our understanding of pathogenesis and could help guide therapy [38]. However, candidates for miRNAs that have the potential to control autoimmune pathogenesis remain limited. Bioinformatics prediction software (Targetscan and miRNA.org) revealed three small molecules that can regulate VDRs as identified *via* a systematic combination of bioinformatics resources [39]. However, we found that only miR-125a-5p was up-regulated and the others were not changed in EAE mice.

MiR-125a-5p is a key regulator of the tight integrity of brain endothelial cells and the egress of migrating immune cells [40, 41]. Studies have shown that miR-125a-5p is down-regulated in systemic lupus erythematosus [42], in oral mucosal disease [43], and in blood samples from pediatric patients with MS [44]. These findings provide a valuable candidate biomarker for some autoimmune diseases. In the present study, we demonstrated for the first time that miR-125a-5p in the spinal ventral horn (lumbar enlargement) is involved in an EAE model induced by MOG. We provided the following supporting evidence: first, miR-125a-5p expression was increased at both the protein and mRNA levels in the ventral horn of the lumbar enlargement of EAE mice; second, and importantly, application of the miR-125a-5p antagomir significantly reduced the clinical symptoms in EAE mice.

So far, how miR-125-5p contributes to the development of autoimmunity is unclear. Some researchers have demonstrated that miR-125a-5p inhibits inflammation by disrupting the differentiation of other effector molecules, thereby stabilizing regulatory T cell commitment and immunoregulation [40, 45]. This finding identified miR-

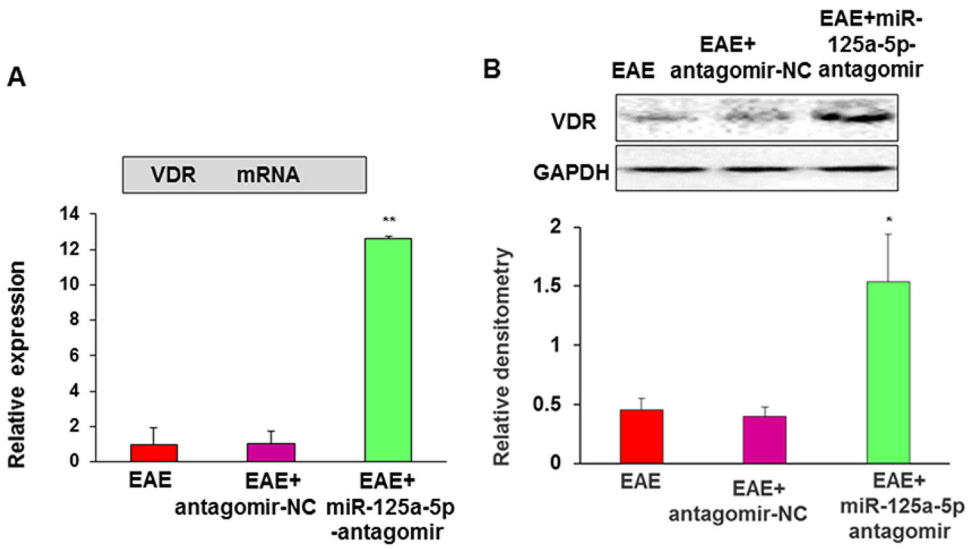

Fig. 9 MiR-125a-5p antagomir enhanced VDR expression. **A** QPCR showed that the VDR mRNA level was significantly higher in EAE mice after intrathecal injection of the miR-125a-5p antagomir than in the antagomir-NC and EAE groups of mice ($n = 4$, $^{**}P < 0.01$, one-way ANOVA). **B** Western blot assays showed that VDR protein expression in EAE mice was significantly higher after intrathecal injection of the miR-125a-5p antagomir than in the antagomir-NC and EAE groups ($n = 4$, $^{*}P < 0.01$, one-way ANOVA).

125a-5p as a key regulator of $CD4^+$ T-cell differentiation that prevents autoimmune pathogenesis by controlling the balance between immune tolerance and the development of autoimmunity [46, 47]. We showed here that miR-125-5p specifically targeted VDRs in the spinal ventral horn; this might be one of mechanisms of MS development, although miR-125a-5p has > 100 targets. We showed that inhibition of miR-125a-5p reversed the pattern of decreased VDR expression at the protein and mRNA levels. Importantly, the results of immunofluorescence analysis and FISH demonstrated that miR-125a-5p was co-localized with VDRs in the same spinal neurons – an observation that indicated the anatomical possibility of the regulation of VDR expression by miR-125a-5p. More importantly, application of the miR-125a-5p antagomir clearly reversed the decreased VDR expression both at the protein and at the mRNA levels.

In summary, we demonstrated that miR-125a-5p/VDR signaling plays a critical role in EAE, and suggested a potential novel therapeutic application in MS and other autoimmune disease states.

Acknowledgements This work was supported by the International Science and Technology Cooperation Plan of Guizhou Province, China [(2013) 7027] and the National Natural Science Foundation of China (81471137 and 31730040).

Conflict of interest The authors declare that they have no competing interests.

References

1. Lau A, Qiu W, Kermode A, Au C, Ng A, Wong A, *et al.* High prevalence and indexes of anti-John Cunningham virus antibodies in a cohort of Chinese patients with multiple sclerosis. Mult Scler J Exp Transl Clin 2018, 4: 2055217318788699.
2. Li WY, Zhang WT, Cheng YX, Liu YC, Zhai FG, Sun P, *et al.* Inhibition of KLF7-targeting MicroRNA 146b promotes sciatic nerve regeneration. Neurosci Bull 2018, 34: 419–437.
3. Zhang Z, Chen W, Zhao Y, Yang Y. Spatiotemporal imaging of cellular energy metabolism with genetically-encoded fluorescent sensors in brain. Neurosci Bull 2018, 34: 875–886.
4. Hauser SL, Oksenberg JR. The neurobiology of multiple sclerosis: genes, inflammation, and neurodegeneration. Neuron 2006, 52: 61–76.
5. Li Z, Li K, Zhu L, Kan Q, Yan Y, Kumar P, *et al.* Inhibitory effect of IL-17 on neural stem cell proliferation and neural cell differentiation. BMC Immunol 2013, 14: 20.
6. Popescu BF, Pirko I, Lucchinetti CF. Pathology of multiple sclerosis: where do we stand? Continuum (Minneap Minn) 2013, 19: 901–921.
7. Lu Y, Zhu ZG, Ma QQ, Su YT, Han Y, Wang X, *et al.* A critical time-window for the selective induction of hippocampal memory consolidation by a brief episode of slow-wave sleep. Neurosci Bull 2018, 34: 1091–1099.
8. Chang Y, Shu Y, Sun X, Xu C, He D, Fang L, *et al.* Ectrodactyly in a Chinese patient born to a mother with neuromyelitis optica spectrum disorder. Mult Scler Relat Disord 2018, 19: 70–72.
9. Butzkueven H, Calabresi PA. Is my MS patient failing treatment? Neurology 2016, 87: 124–125.
10. Giovannoni G, Butzkueven H, Dhib-Jalbut S, Hobart J, Kobelt G, Pepper G, *et al.* Brain health: time matters in multiple sclerosis. Mult Scler Relat Disord 2016, 9 Suppl 1: S5–S48.
11. Ascherio A, Munger KL, Simon KC. Vitamin D and multiple sclerosis. Lancet Neurol 2010, 9: 599–612.
12. Burden of illness of multiple sclerosis: Part II: Quality of life. The Canadian burden of illness study group. Can J Neurol Sci 1998, 25: 31–38.
13. Jiao KP, Li SM, Lv WY, Jv ML, He HY. Vitamin D3 repressed astrocyte activation following lipopolysaccharide stimulation in vitro and in neonatal rats. Neuroreport 2017, 28: 492–497.
14. Boontanrart M, Hall SD, Spanier JA, Hayes CE, Olson JK. Vitamin D3 alters microglia immune activation by an IL-10 dependent SOCS3 mechanism. J Neuroimmunol 2016, 292: 126–136.
15. Baeke F, Takiishi T, Korf H, Gysemans C, Mathieu C. Vitamin D: modulator of the immune system. Curr Opin Pharmacol 2010, 10: 482–496.
16. Takahashi K, Nakayama Y, Horiuchi H, Ohta T, Komoriya K, Ohmori H, *et al.* Human neutrophils express messenger RNA of vitamin D receptor and respond to 1alpha,25-dihydroxyvitamin D3. Immunopharmacol Immunotoxicol 2002, 24: 335–347.
17. Yang JT, Wang ZJ, Cai HY, Yuan L, Hu MM, Wu MN, *et al.* Sex differences in neuropathology and cognitive behavior in APP/PS1/tau triple-transgenic mouse model of Alzheimer's disease. Neurosci Bull 2018, 34: 736–746.
18. Penna G, Adorini L. 1 Alpha,25-dihydroxyvitamin D3 inhibits differentiation, maturation, activation, and survival of dendritic cells leading to impaired alloreactive T cell activation. J Immunol 2000, 164: 2405–2411.
19. Sazci A, Uren N, Idrisoglu HA, Ergul E. The rs2228570 variant of the Vitamin D receptor gene is associated with essential tremor. Neurosci Bull 2019, 35: 362–364.
20. Sochorova K, Budinsky V, Rozkova D, Tobiasova Z, Dusilova-Sulkova S, Spisek R, *et al.* Paricalcitol (19-nor-1,25-dihydroxyvitamin D2) and calcitriol (1,25-dihydroxyvitamin D3) exert potent immunomodulatory effects on dendritic cells and inhibit induction of antigen-specific T cells. Clin Immunol 2009, 133: 69–77.
21. Gonzalez-Mateo GT, Fernandez-Millara V, Bellon T, Liappas G, Ruiz-Ortega M, Lopez-Cabrera M, *et al.* Paricalcitol reduces peritoneal fibrosis in mice through the activation of regulatory T cells and reduction in IL-17 production. PLoS One 2014, 9: e108477.
22. Campos-Melo D, Hawley ZCE, Strong MJ. Dysregulation of human NEFM and NEFH mRNA stability by ALS-linked miRNAs. Mol Brain 2018, 11: 43.
23. Oakes JA, Davies MC, Collins MO. TBK1: a new player in ALS linking autophagy and neuroinflammation. Mol Brain 2017, 10: 5.
24. Wu R, Zhang PA, Liu X, Zhou Y, Xu M, Jiang X, *et al.* Decreased miR-325-5p contributes to visceral hypersensitivity through post-transcriptional upregulation of CCL2 in rat dorsal root ganglia. Neurosci Bull 2019. https://doi.org/10.1007/s12264-019-00372-x.
25. Ambros V. The functions of animal microRNAs. Nature 2004, 431: 350–355.
26. Nicoloso MS, Spizzo R, Shimizu M, Rossi S, Calin GA. MicroRNAs–the micro steering wheel of tumour metastases. Nat Rev Cancer 2009, 9: 293–302.
27. Guerau-de-Arellano M, Alder H, Ozer HG, Lovett-Racke A, Racke MK. miRNA profiling for biomarker discovery in multiple sclerosis: from microarray to deep sequencing. J Neuroimmunol 2012, 248: 32–39.

28. Junker A, Hohlfeld R, Meinl E. The emerging role of microRNAs in multiple sclerosis. Nat Rev Neurol 2011, 7: 56–59.
29. Li X, Kroin JS, Kc R, Gibson G, Chen D, Corbett GT, *et al.* Altered spinal microRNA-146a and the microRNA-183 cluster contribute to osteoarthritic pain in knee joints. J Bone Miner Res 2013, 28: 2512–2522.
30. Pan W, Zhu S, Dai D, Liu Z, Li D, Li B, *et al.* MiR-125a targets effector programs to stabilize Treg-mediated immune homeostasis. Nat Commun 2015, 6: 7096.
31. Su S, Shao J, Zhao Q, Ren X, Cai W, Li L, *et al.* MiR-30b attenuates neuropathic pain by regulating voltage-gated sodium channel Nav1.3 in rats. Front Mol Neurosci 2017, 10: 126.
32. Becher B, Durell BG, Noelle RJ. Experimental autoimmune encephalitis and inflammation in the absence of interleukin-12. J Clin Invest 2002, 110: 493–497.
33. Garay L, Gonzalez Deniselle MC, Lima A, Roig P, De Nicola AF. Effects of progesterone in the spinal cord of a mouse model of multiple sclerosis. J Steroid Biochem Mol Biol 2007, 107: 228–237.
34. Fraga-Silva TF, Mimura LA, Zorzella-Pezavento SF, Ishikawa LL, Franca TG, Thome R, *et al.* Tolerogenic vaccination with MOG/VitD overcomes aggravating effect of C. albicans in experimental encephalomyelitis. CNS Neurosci Ther 2016, 22: 807–816.
35. Smolders J, Menheere P, Kessels A, Damoiseaux J, Hupperts R. Association of vitamin D metabolite levels with relapse rate and disability in multiple sclerosis. Mult Scler 2008, 14: 1220–1224.
36. Munger KL, Aivo J, Hongell K, Soilu-Hanninen M, Surcel HM, Ascherio A. Vitamin D status during pregnancy and risk of multiple sclerosis in offspring of women in the finnish maternity cohort. JAMA Neurol 2016, 73: 515–519.
37. Munger KL, Levin LI, Hollis BW, Howard NS, Ascherio A. Serum 25-hydroxyvitamin D levels and risk of multiple sclerosis. JAMA 2006, 296: 2832–2838.
38. Abidin AZ, Chockanathan U, AM DS, Inglese M, Wismuller A. Using large-scale granger causality to study changes in brain network properties in the clinically isolated syndrome (CIS) stage of multiple sclerosis. Proc SPIE Int Soc Opt Eng 2017, 10137.
39. Wang Y, Yang Z, Le W. Tiny but mighty: Promising roles of microRNAs in the diagnosis and treatment of Parkinson's disease. Neurosci Bull 2017, 33: 543–551.
40. Zhang J, Shi K, Li Z, Li M, Han Y, Wang L, *et al.* Organ- and cell-specific immune responses are associated with the outcomes of intracerebral hemorrhage. FASEB J 2018, 32: 220–229.
41. Mo JL, Pan ZG, Chen X, Lei Y, Lv LL, Qian C, *et al.* MicroRNA-365 knockdown prevents ischemic neuronal injury by activating oxidation resistance 1-mediated antioxidant signals. Neurosci Bull 2019. https://doi.org/10.1007/s12264-019-00371-y.
42. Zhao X, Tang Y, Qu B, Cui H, Wang S, Wang L, *et al.* MicroRNA-125a contributes to elevated inflammatory chemokine RANTES levels via targeting KLF13 in systemic lupus erythematosus. Arthritis Rheum 2010, 62: 3425–3435.
43. Hu JY, Zhang J, Cui JL, Liang XY, Lu R, Du GF, *et al.* Increasing CCL5/CCR5 on CD4 + T cells in peripheral blood of oral lichen planus. Cytokine 2013, 62: 141–145.
44. Liguori M, Nuzziello N, Licciulli F, Consiglio A, Simone M, Viterbo RG, *et al.* Combined microRNA and mRNA expression analysis in pediatric multiple sclerosis: an integrated approach to uncover novel pathogenic mechanisms of the disease. Hum Mol Genet 2018, 27: 66–79.
45. Wang J, Li X, Zhang DQ, Yang CS, Qi Y, Li MS, *et al.* Quantitative analysis of aquaporin-4 antibody in longitudinally extensive transverse myelitis. J Neuroimmunol 2015, 278: 26–29.
46. Maldonado RA, Irvine DJ, Schreiber R, Glimcher LH. A role for the immunological synapse in lineage commitment of CD4 lymphocytes. Nature 2004, 431: 527–532.
47. O'Shea JJ, Paul WE. Mechanisms underlying lineage commitment and plasticity of helper CD4 + T cells. Science 2010, 327: 1098–1102.